This manuscript is a preprint and has not been peer reviewed. The copyright holder has made the manuscript available under a Creative Commons Attribution 4.0 International (CC BY) license and consented to have it forwarded to EarthArXiv for public posting.

Increasing national annual rainfall alongside trends in Kenya's equatorial bimodal rainy seasons and recurrent lower-tail years, 2000–2024: dependence-aware analysis with exploratory 1991–1999 context

Kenya's annual and bimodal seasonal rainfall trends, 1991-2024

Research Article

Solomon M. Nzioka[1]*, Bosco L. Lolem[2], Emmanuel Wamalwa[3], Jeremiah Mushosho[4]

[1] Phoenix Climate and Health Impact Experts, Nairobi, Kenya
[2] Climate Change and Health Unit, Ministry of Health, Nairobi, Kenya
[3] Department of Public Health, Daystar University, Nairobi, Kenya
[4] Climate Change, Health and Environment, WHO Regional Office for Africa, Brazzaville, Republic of the Congo
Corresponding author: Solomon M. Nzioka | solomonmn@climate-health-impacts.net | ORCID: 0009-0004-7915-1270

Abstract

National annual rainfall trends can conceal seasonal changes relevant to water availability and climate-sensitive health risks. This study examined whether increasing national rainfall in Kenya was reflected consistently across its two principal rainy seasons, March–May (MAM) and October–December (OND), and whether seasonal lower-tail years coincided. The analysis covered 2000–2024, with 1991–1999 examined separately as exploratory historical context. Trends were estimated using Theil–Sen slopes, Newey–West heteroskedasticity- and autocorrelation-consistent (HAC) regression, and circular block bootstrapping. Complementary one-sided tests assessed directional rainfall increases, while season-specific empirical twentieth-percentile thresholds identified lower-tail seasons.

National annual rainfall increased by 78.25 mm per decade (95% block-bootstrap confidence interval [CI]: 43.74–102.91; HAC p=0.0103). Three annual totals were at or below the empirical 10th-percentile threshold and five at or below the 20th percentile. MAM rainfall increased by 28.66 mm per decade (95% block-bootstrap CI: 7.55–40.78; two-sided HAC p=0.0266), with directional support across tested HAC lags and bootstrap block lengths (one-sided p=0.0164), although the Holm-adjusted two-sided result was just above the 0.05 threshold (p=0.0532). OND had a smaller positive trend estimate of 14.65 mm per decade (95% block-bootstrap CI: −2.28 to 31.03; two-sided p=0.0707). Its directional result was supported under primary settings (p=0.0411), but was not robust across sensitivity settings. Five MAM (20%) and five OND (20%) seasons fell below their respective empirical twentieth-percentile thresholds, with no year experiencing deficits in both seasons.

The findings reveal that increasing national annual rainfall does not translate into uniform seasonal rainfall increases or eliminate recurrent seasonal deficits. Evidence of an increase was stronger for MAM than OND. This seasonally differentiated evidence provides a basis for climate–health vulnerability assessments that integrate rainfall dynamics with the spatial distribution of populations exposed to climate hazards; health outcomes were not directly assessed.

Keywords: Kenya; CHIRPS; annual precipitation; rainfall variability; lower-tail rainfall; drought monitoring; Theil–Sen; moving-block bootstrap; autocorrelation.

This manuscript is a preprint and has not been peer reviewed. The copyright holder has made the manuscript available under a Creative Commons Attribution 4.0 International (CC BY) license and consented to have it forwarded to EarthArXiv for public posting.

1. Introduction

Rainfall is a principal control on water availability, agricultural production, pastoral livelihoods, ecosystem function and the operation of essential services across eastern Africa. Its consequences depend not only on the annual amount received, but also on when rainfall occurs, how it is distributed between seasons and whether deficits persist long enough to affect soil moisture, water storage and livelihoods. A national annual total is therefore useful, but incomplete, as a description of drought-related conditions.

Rainfall behaviour in eastern Africa is spatially and seasonally heterogeneous. The March–May long rains and October–December short rains have different circulation controls and have not followed a single regional trajectory. Reviews describe long-rains drying over parts of eastern Africa during particular periods, alongside wetter short-rains tendencies and strong interannual modulation by ocean–atmosphere variability [1,2].

The long-rains decline has also been associated with later onset and earlier cessation, rather than a uniform reduction in peak rainfall intensity [3]. Satellite-product comparisons likewise show that inferred trends depend on the rainfall product, geographic domain and precipitation metric [4]. Kenyan county-level evidence has documented wetting and drying anomalies in both rainy seasons and increased rainfall variability [5]. These findings make it inappropriate to infer a uniform local response from a national annual trend.

Gridded precipitation products support climate analysis where rain-gauge networks are sparse or uneven. CHIRPS combines infrared satellite information, climatology and station observations to provide a long-term precipitation record at relatively fine spatial and temporal resolution [6]. Validation over eastern Africa supports its regional utility but also identifies spatial differences in performance, including weaker performance in some coastal and mountainous settings [7]. The data source, aggregation method and analytical uncertainty are therefore accompanying the reported trend estimates.

A positive annual rainfall trend is sometimes interpreted as evidence that drought has become less frequent or less consequential. That inference should not follow from annual totals alone. Annual accumulation can increase while one rainy season becomes drier or shorter, if another season becomes wetter or a small number of intense events contribute more to the annual sum. Annual precipitation amount and the occurrence of lower-tail annual totals are related, but distinct, quantities.

This study examined national annual rainfall trends in Kenya alongside changes in the country's two principal bimodal rainy seasons, March–May (MAM) and October–December (OND), during 2000–2024. It addressed four related objectives: (i) to quantify the direction and magnitude of national annual rainfall change and determine whether lower-tail annual rainfall years continued to occur; (ii) to estimate MAM and OND rainfall accumulation trends independently and assess the strength and robustness of evidence for directional increases; (iii) to evaluate changes in the relative behaviour of the two rainy seasons through paired comparisons of their estimated trend rates and the temporal trend in their annual MAM–OND rainfall accumulation gap; and (iv) to characterise season-specific rainfall deficits using empirical twentieth-percentile (P20) thresholds and examine their occurrence and concurrence within calendar years.

The principal analysis used the 2000–2024 CHIRPS record. A separate 1991–1999 national rainfall series was examined as exploratory historical context, with estimates retained independently and without pooling across the source transition. Annual and seasonal trends were assessed using Theil–Sen estimation, circular moving-block residual bootstrapping and Newey–West heteroskedasticity- and autocorrelation-consistent (HAC) inference. Complementary one-sided tests evaluated directional evidence of increasing seasonal rainfall, while paired analyses distinguished changes in individual seasonal trends from changes in the annual difference between MAM and OND. This integrated approach distinguishes national annual rainfall change, season-specific trend evidence and the occurrence of lower-tail seasonal conditions, providing a more differentiated basis for interpreting rainfall variability and its relevance to climate-risk and climate–health vulnerability assessment.

This manuscript is a preprint and has not been peer reviewed. The copyright holder has made the manuscript available under a Creative Commons Attribution 4.0 International (CC BY) license and consented to have it forwarded to EarthArXiv for public posting.

2. Materials and Methods

2.1 Study period and rainfall data

The principal inferential period covered January 2000 to December 2024. The annual CHIRPS series comprised 25 complete national observations derived from 300 monthly CHIRPS version 2.0 precipitation records. CHIRPS v2.0 has a nominal spatial resolution of 0.05° × 0.05° (approximately 5 km) [6,8].

A separate historical national rainfall series covered January 1991 to December 1999, comprising 108 monthly observations and nine annual observations. It was extracted from the January 1991–December 1999 subset of the Kenya Climate Data | 1991–2016 rainfall dataset catalogued by Code for Africa on openAFRICA [9]. The analytical historical input is a national tabular series without spatial coordinates, raster-cell identifiers or county-level fields. Its upstream grid resolution and aggregation procedure is linked to World Bank CCKP CRU TS 4.07 in its contextual catalogue metadata [10]. As the provenance of the openAFRICA tabular form could not be independently established, the two source periods were therefore retained separately and were not homogenised or pooled for trend estimation or formal cross-era hypothesis testing. Source characteristics and spatial support are summarised in Supplementary Table S1.

2.2 Spatial extraction and national rainfall aggregation

Monthly CHIRPS precipitation was extracted from the native approximately 0.05° geographic grid (EPSG:4326), without resampling or reprojection. Kenya's national boundary and 47 county polygons defined the spatial extraction support. A boundary-inclusive cell-selection procedure retained raster cells intersecting the relevant administrative polygons, including partial boundary cells, using their complete native rainfall values without fractional-area adjustment.

For each month, national rainfall was calculated as the arithmetic mean of all valid CHIRPS pixel values selected within the national spatial mask. The resulting estimator was pixel-count weighted, rather than geographically area weighted or population weighted:

$$\overline{R}_t = \frac{1}{N_t}\sum_{i=1}^{N_t} R_{i,t}$$

where $\overline{R}_t$ is the national mean-pixel rainfall for month t, $R_{i,t}$ is the rainfall value of valid pixel i, and N_t is the number of valid pixels in that month.

NoData cells were excluded from the numerator and valid-pixel denominator; they were not treated as zero rainfall or imputed. The valid-pixel count was retained for each monthly observation and was constant at 18,896 across the 300 CHIRPS months.

County rainfall estimates were calculated independently from their respective valid native-grid pixels. The national series was derived directly from the national spatial mask and was not reconstructed by averaging county means. The national annual and seasonal analyses reported here use the national rainfall series; county-level exposure and population overlays were not estimated in this study.

2.3 Annual and seasonal rainfall series construction

Monthly rainfall values were aggregated into calendar-year annual totals by summing the 12 monthly observations within each year:

$$A_y = \sum_{m=1}^{12} \overline{R}_{y,m}$$

This manuscript is a preprint and has not been peer reviewed. The copyright holder has made the manuscript available under a Creative Commons Attribution 4.0 International (CC BY) license and consented to have it forwarded to EarthArXiv for public posting.

where A_y is annual national rainfall in year y, and $\overline{R}_{y,m}$ is the national mean-pixel rainfall for month m of that year. The resulting series comprised 25 annual observations for 2000–2024 and nine separate historical observations for 1991–1999.

Two principal rainy-season accumulation series were derived independently for each source period. March–May (MAM) rainfall was calculated as the sum of national monthly rainfall in March, April and May, while October–December (OND) rainfall was calculated as the sum in October, November and December:

$$MAM_y = \sum_{m=3}^{5} \overline{R}_{y,m}$$

$$OND_y = \sum_{m=10}^{12} \overline{R}_{y,m}$$

Each source period therefore yielded paired annual MAM and OND observations: nine paired years for 1991–1999 and 25 paired years for 2000–2024. Seasonal totals are expressed in millimetres per season.

The historical and CHIRPS seasonal series were constructed and analysed independently. No pooled seasonal series, pooled trend estimate or formal hypothesis test comparing the two source periods was undertaken. Alternative annual rainfall representations, including mean monthly rainfall and absolute, percentage and standardised anomalies, were treated as transformations of the same annual observations rather than independent inferential outcomes.

2.4 Trend estimation and dependence-aware inference

Theil–Sen estimation was used to quantify the magnitude and direction of annual and seasonal rainfall trends. The estimator is based on the median of pairwise slopes and is reported in millimetres per decade [11,12]:

$$\widehat{\beta_{Sen}} = 10 \times median\left(\frac{Y_j - Y_i}{t_j - t_i}\right), \qquad i < j$$

Where Y_j and Y_i are the observed rainfall values at calendar years t_j and t_i, respectively. Kendall's tau-b was additionally used to describe monotonic association between calendar year and annual rainfall [13].

a) *Residual circular moving-block bootstrap;* uncertainty in Theil–Sen slope estimates was assessed using residual circular moving-block bootstrap (CBB) procedures. A linear trend was fitted to each series, and contiguous blocks of its detrended residuals were resampled with circular indexing. Resampled residuals were added to the fitted trend, and the Theil–Sen slope was re-estimated for each replicate.

The fitted trend and residual representation was:

$$Y_t = \hat{Y}_t + e_t$$

Where $\hat{Y}_t$ is the fitted linear trend and e_t is the corresponding residual. For bootstrap replicate b:

$$Y_t^{*(b)} = \hat{Y}_t + e_t^{*(b)}$$

where $e_t^{*(b)}$ represents the residual sequence reconstructed by circular block resampling.

This manuscript is a preprint and has not been peer reviewed. The copyright holder has made the manuscript available under a Creative Commons Attribution 4.0 International (CC BY) license and consented to have it forwarded to EarthArXiv for public posting.

The primary analysis used 10,000 bootstrap replicates with a five-year block length. Three- and seven-year blocks were examined as sensitivity specifications. The 95% percentile confidence interval was defined by the 2.5th and 97.5th percentiles of the bootstrap slope distribution [14,15]:

$$CI_{95\%} = [Q_{0.025}(\hat{\beta}^*), Q_{0.975}(\hat{\beta}^*)]$$

b) Heteroskedasticity- and autocorrelation-consistent regression (HAC); a complementary ordinary least-squares regression estimated the linear temporal trend using Newey–West HAC covariance estimation [16]:

$$Y_t = \alpha + \beta(t - \bar{t}) + \varepsilon_t$$

where Y_t is annual or seasonal rainfall, α is the intercept, β is the annual linear trend coefficient, $\bar{t}$ is the mean observation year, and ε_t is the regression error. HAC inference was used to account for heteroskedasticity and serial correlation in the regression errors.

The primary HAC specification used a two-year lag, with one- and three-year lags assessed for sensitivity. A t-based reference distribution was used for confidence intervals and hypothesis tests. The coefficient of determination R^2 was reported descriptively and was not used as a criterion for trend significance.

For the seasonal analysis, four independent within-era models were fitted: MAM and OND for 1991–1999, and MAM and OND for 2000–2024. The primary CBB and HAC settings were applied consistently across these models. The nine-year historical estimates were treated as exploratory because of the limited number of annual observations and the resulting uncertainty in dependence-aware inference.

c) Multiplicity adjustment; two-sided HAC p-values for the MAM and OND trend models were adjusted for multiple comparisons using the Holm procedure separately within each source era. Thus, the two seasonal tests were corrected within 1991–1999 and independently within 2000–2024; no correction or hypothesis test was performed across eras.

Complementary directional analysis. Separate one-sided tests evaluated evidence of increasing seasonal rainfall, using the directional hypotheses:

$$H_0: \beta \leq 0$$
$$H_1: \beta > 0$$

Directional HAC inference was evaluated using the primary two-year lag and alternative one- and three-year lags. Directional bootstrap lower confidence bounds were also examined across the five-year primary and three- and seven-year sensitivity block lengths. These one-sided results were reported separately from the two-sided seasonal tests and their Holm-adjusted p-values; they were not included in the Holm correction. Their interpretation as confirmatory evidence depends on whether the directional hypotheses were specified independently of the observed trend results.

2.5 Paired MAM–OND comparative analyses

Two distinct paired estimands were used to examine the relationship between MAM and OND rainfall accumulation. Calendar year was the pairing unit, and both analyses were conducted independently within the 1991–1999 and 2000–2024 source periods.

a) Difference between seasonal trend rates; the first estimand was the difference between the separately estimated seasonal Theil–Sen slopes:

$$\Delta\beta = Sen(MAM) - Sen(OND)$$

This manuscript is a preprint and has not been peer reviewed. The copyright holder has made the manuscript available under a Creative Commons Attribution 4.0 International (CC BY) license and consented to have it forwarded to EarthArXiv for public posting.

This quantity assesses whether the estimated MAM and OND trend rates differ. Its uncertainty was evaluated using a joint paired residual circular moving-block bootstrap. The same resampled calendar-year block indices were applied to the MAM and OND residual vectors, preserving their contemporaneous cross-season pairing. The analysis used 10,000 replicates, a five-year primary block length, and three- and seven-year sensitivity blocks. The primary result was reported as the paired 95% CBB confidence interval for the difference in seasonal slopes.

b) Trend in the signed annual seasonal gap; the second estimand examined the temporal trend in the annual paired difference:

$$D_t = MAM_t - OND_t$$

The Theil–Sen slope of D_t estimated change in the signed additive MAM–OND rainfall gap over time:

$$\widehat{\beta_D} = Sen(D_t)$$

Its uncertainty was assessed using a residual CBB with 10,000 replicates, a five-year primary block length and three- and seven-year sensitivity specifications. A complementary two-sided HAC regression tested the temporal trend in D_t, using a two-year primary lag and one- and three-year sensitivity lags:

$$D_t = \alpha_D + \beta_D\left(t - \bar{t}\right) + \varepsilon_{D,t}$$

These estimands answer different questions. The difference between the separate seasonal Sen slopes, $Sen(MAM) - Sen(OND)$ is not generally equivalent to the Sen slope of the annual signed difference, $Sen(MAM - OND)$. The latter represents an additive difference in millimetres; it is neither the unsigned magnitude of the seasonal gap nor a comparison of proportional rainfall shares. Both estimands were interpreted within their respective source periods, without pooling or cross-era testing.

2.6 Annual empirical lower-tail thresholds and classification

Annual rainfall P10 and P20 thresholds were estimated independently within each source period using linear empirical quantile interpolation:

$$P10 = Q_{0.10}(A_y)$$
$$P20 = Q_{0.20}(A_y)$$

where A_y represents the annual rainfall observations within the relevant source period. The thresholds therefore describe the lower tail of each source-era annual rainfall distribution rather than externally prescribed drought thresholds.

Annual observations were classified into three mutually exclusive categories:

$$C_y = \begin{cases} 1, & A_y < P10 \\ 2, & P10 < A_y \leq P20 \\ 3, & A_y > P20 \end{cases}$$

These inclusive boundaries ensured that every annual observation belonged to exactly one category. Annual counts and proportions were reported descriptively. Uncertainty in the estimated thresholds and associated annual proportions was assessed using circular moving-block bootstrap resampling, with a five-year primary block length. No p-values were assigned to frequencies derived from thresholds estimated from the same observations.

For frequency reporting, years strictly below each threshold were identified using $(R_y < P10)$ and $(R_y < P20)$, respectively. For mutually exclusive annual classification, inclusive boundary rules were applied: P10 or lower $(R_y \leq P10)$; above P10 through P20 $(P10 < R_y \leq P20)$; and above P20 $(R_y > P20)$. This distinction preserves a complete, non-overlapping classification, including any observation exactly equal to an estimated threshold. The threshold estimation and annual classification procedures are summarised in Figure 1.

This manuscript is a preprint and has not been peer reviewed. The copyright holder has made the manuscript available under a Creative Commons Attribution 4.0 International (CC BY) license and consented to have it forwarded to EarthArXiv for public posting.

Uncertainty in the seasonal deficit frequencies and threshold estimates and associated annual proportions was assessed using 10,000 paired-year circular moving-block bootstrap replicates, with a five-year primary block length. MAM and OND indicators were resampled together using the same calendar-year block indices, preserving their annual pairing. For each replicate, the corresponding event frequency was recalculated from the resampled paired observations. The resulting percentile 95% confidence intervals were conditional on the season-specific P20 thresholds estimated from the full source-era series; threshold-estimation uncertainty was not propagated. Given the nine-year historical sample, its seasonal deficit frequencies and bootstrap intervals were treated as exploratory. No p-values were assigned to frequencies derived from thresholds estimated from the same 25 annual observations.

2.7 Statistical reporting, software and reproducibility

Geospatial preprocessing and raster operations were undertaken using the Ubuntu system Python 3.14.4. Raster processing and data access used Rasterio 1.5.1 and GDAL 3.12.2; vector and spatial data operations used GeoPandas 1.2.0, Shapely 2.1.2, pyproj 3.8.0, affine 3.0.1 and pyogrio 0.13.0. The associated geospatial libraries included GEOS 3.13.1 and PROJ 9.8.1, as reported by Shapely and pyproj, respectively. The system environment additionally included NumPy 2.3.5, pandas 3.0.6 and SciPy 1.16.3. Statistical analyses were conducted in a separate Python 3.14.4 CHRIS virtual environment. Numerical computation and array operations used NumPy 2.5.4; tabular data management used pandas 3.1.0; statistical estimation, including Theil–Sen trend estimation, used SciPy 1.18.1; and regression modelling with heteroskedasticity- and autocorrelation-consistent covariance estimation used statsmodels 0.15.0. The virtual environment included Matplotlib 3.11.2 and Pillow 13.0.0 for figure generation and image processing. Both environments operated on a 64-bit Ubuntu Linux platform under WSL2, using Linux kernel 6.6.87.2-microsoft-standard-WSL2 and glibc 2.43.

The analysis code, source-separated monthly national rainfall inputs, derived annual and seasonal series, machine-readable statistical results, data dictionaries, provenance documentation and quality-assurance manifests are archived in Zenodo (https://doi.org/10.5281/zenodo.23951555). The package reproduces the analytical workflow from the governed national monthly rainfall input series onward; it does not contain the original CHIRPS GeoTIFF archive or the upstream raster-to-national aggregation workflow.

3. Results

3.1 Exploratory historical rainfall profile, 1991–1999

The nine-year historical series shows substantial interannual variability and an exploratory upward tendency. Its Theil–Sen slope was approximately +134.19 mm per decade. The series includes an unusually wet year in 1997, while 1991 and 1996 fall within the source-era lower tail. Given the short record and the historical series' unresolved upstream grid provenance, this slope is descriptive and is not directly comparable with the CHIRPS estimate.

Against the historical source's empirical thresholds, one year (1996; 11.1%) was at or below P10 and two years (1991 and 1996; 22.2%) were at or below P20. Thus, one year (1991; 11.1%) fell above P10 and at or below P20, while seven years (77.8%) were above P20. Eight of nine years (88.9%) were above P10. These categories identify relative annual deficits within the short source-era distribution, not drought duration or seasonal severity. The 1991–1999 historical rainfall series is not combined with the CHIRPS period for inferential trend estimation.

3.2 National annual rainfall trend, 2000–2024

January 2000 marks the transition to the principal CHIRPS series. The short nine-year historical segment is useful for contextual description only. It was not used to infer a like-for-like change in annual rainfall trend between the two source eras.

This manuscript is a preprint and has not been peer reviewed. The copyright holder has made the manuscript available under a Creative Commons Attribution 4.0 International (CC BY) license and consented to have it forwarded to EarthArXiv for public posting.

The primary five-year circular moving-block bootstrap 95% confidence interval was 43.74–102.91 mm per decade. The complementary HAC regression estimated an increase of 80.86 mm per decade (SE 28.96; 95% CI 20.96–140.76; p=0.0103). Kendall's tau-b was 0.273, and the R^2 was 0.211.

Table 1: National annual rainfall trend and primary inference, Kenya, 2000–2024.

Measure	Estimate
Annual observations	25 (2000–2024)
Mean annual rainfall	640.08 mm
Annual standard deviation	129.42 mm
Theil–Sen slope	+78.25 mm/decade
Theil–Sen 95% circular block-bootstrap CI	43.74 to 102.91 mm/decade
HAC linear slope	+80.86 mm/decade
HAC standard error	28.96
HAC 95% CI	20.96 to 140.76 mm/decade
HAC p-value (two-year lag)	0.0103
Kendall's tau-b	0.273
OLS R^2	0.211

The trend direction remained positive across the evaluated bootstrap block lengths and HAC lag specifications. Alternative displayed representations produced Theil–Sen slopes of +78.25 mm per decade for annual rainfall and absolute anomalies, +6.52 mm per month per decade for mean monthly rainfall, +12.22 percentage points per decade for percentage anomalies, and +0.605 standard deviations per decade for standardised anomalies. Their shared p-value reflects the same underlying annual observations, not independent confirmations.

Table 2: Alternative representations of the same national rainfall trend; these are not independent tests.

Representation	Theil–Sen slope per decade	95% bootstrap CI	HAC p-value
Annual rainfall	+78.25 mm	43.74 to 102.91 mm	0.0103
Annual mean monthly rainfall	+6.52 mm/month	3.64 to 8.58 mm/month	0.0103
Absolute rainfall anomaly	+78.25 mm	43.74 to 102.91 mm	0.0103
Percentage anomaly	+12.22 percentage points	6.83 to 16.08	0.0103
Standardised anomaly	+0.605 SD	0.338 to 0.795 SD	0.0103

Figure 2 illustrates annual rainfall variability, the separation between the two source periods and the source-era-specific empirical lower-tail classifications.

3.3 Robustness to dependence specifications

The positive Theil–Sen estimate persisted across all three bootstrap block lengths. The primary five-year interval and the repeated five-year sensitivity calculation were identical after removal of a duplicated earlier calculation. The direction and statistical support of the HAC trend were also retained across the one-, two- and three-year lag specifications.

Table 3: Moving-block bootstrap sensitivity to block length

Specification	Slope (mm/decade)	95% CI
Circular bootstrap, 3-year blocks	+78.25	17.43 to 125.23
Circular bootstrap, 5-year blocks (primary)	+78.25	43.74 to 102.91
Circular bootstrap, 7-year blocks	+78.25	37.97 to 103.37

Table 4: Newey–West HAC lag sensitivity

HAC lag	Slope (mm/decade)	SE	95% CI	p-value
1 year	+80.86	34.61	9.27 to 152.45	0.0285
2 years (primary)	+80.86	28.96	20.96 to 140.76	0.0103
3 years	+80.86	22.41	34.50 to 127.22	0.0015

This manuscript is a preprint and has not been peer reviewed. The copyright holder has made the manuscript available under a Creative Commons Attribution 4.0 International (CC BY) license and consented to have it forwarded to EarthArXiv for public posting.

As shown in Figure 3, all evaluated bootstrap confidence intervals excluded zero, and all HAC p-values were below 0.05. This agreement supports a positive trend within the tested specifications. It does not remove uncertainty arising from the short annual record, the selected precipitation product or the untested forms of temporal variability.

3.4 Lower-tail rainfall thresholds and dry-year frequency

The empirical P10 threshold was 514.04 mm (95% bootstrap CI 444.31–540.12 mm), and the P20 threshold was 536.90 mm (95% bootstrap CI 513.72–573.45 mm). Three of the 25 annual observations (12%) were at or below P10. Five (20%) were at or below P20, comprising the three P10 years and two additional years between P10 and P20. The remaining 20 observations (80%) were above P20 as shown in Table 5 and Figure 4.

Table 5: Empirical lower-tail annual rainfall thresholds and mutually exclusive frequencies, Kenya, 2000–2024

Threshold/category	Rainfall threshold or count	Observed share	95% bootstrap interval
P10 threshold	514.04 mm	—	444.31 to 540.12 mm
P20 threshold	536.90 mm	—	513.72 to 573.45 mm
At or below P10	3/25	12%	4% to 20%
Above P10 to P20	2/25	8%	0% to 16%
Above P20	20/25	80%	64% to 92%

The lower-tail classifications demonstrate that a positive long-term annual trend coexisted with relatively dry years. Their frequencies describe the realised distribution against sample-derived cut-offs; they are not a separate hypothesis test of a change in drought frequency or severity.

3.5 Complementary Rainfall Seasonality comparative analytics

The seasonal analysis examined two related but distinct aspects of Kenya's bimodal rainfall regime: whether MAM and OND rainfall accumulation exhibited different temporal trend rates, and whether the annual difference between their accumulations changed over time. These questions were addressed using the difference between their independently estimated Theil–Sen slopes, Sen(MAM) − Sen(OND), and the Theil–Sen trend in their annual paired difference, Sen(MAM − OND), respectively.

Two distinct estimands were examined to assess the relationship between MAM and OND rainfall accumulation, with inference based on circular moving-block bootstrap (CBB) procedures. The first assessed the difference in seasonal trend rates, calculated as the difference between the separately estimated Theil–Sen slopes, Sen(MAM) − Sen(OND). Its uncertainty was evaluated using a joint paired residual CBB, with the 95% confidence interval (CI) providing inference on whether the estimated seasonal trend rates differed.

The second assessed temporal change in the annual seasonal rainfall gap, defined as the annual paired difference between MAM and OND rainfall accumulation (MAM − OND). The Theil–Sen slope of this annual difference quantified whether the relative accumulation gap changed over time. Inference combined the residual CBB 95% CI with a two-sided Newey–West heteroskedasticity- and autocorrelation-consistent (HAC) test.

Both analyses used 10,000 bootstrap replicates, with 3-, 5- and 7-year block lengths evaluated for sensitivity. For the annual MAM–OND gap analysis, HAC sensitivity was additionally assessed using 1-, 2- and 3-year lags. Figure 5 presents the trends and the results from the two estimands.

This manuscript is a preprint and has not been peer reviewed. The copyright holder has made the manuscript available under a Creative Commons Attribution 4.0 International (CC BY) license and consented to have it forwarded to EarthArXiv for public posting.

Panels A–B: Temporal trends in the signed annual MAM–OND rainfall accumulation gap. The annual contrast is calculated as MAM minus OND seasonal rainfall accumulation (mm/season). Points represent observed annual differences, dashed lines indicate within-era Theil–Sen trends, and the horizontal dotted line denotes zero difference. Annotations report the Theil–Sen slope, 95% residual circular moving-block bootstrap (CBB) confidence interval, HAC regression slope and confidence interval, and two-sided HAC p-value (Newey–West lag 2).

Panels C–D: Individual seasonal rainfall trajectories and differences in trend rates. Blue and green series represent observed MAM and OND seasonal rainfall accumulation, respectively, with corresponding dashed lines showing independent within-era Theil–Sen trends. Annotations provide season-specific slope estimates and 95% residual CBB confidence intervals. The difference between seasonal trend rates is calculated as Sen(MAM) minus Sen(OND), with uncertainty estimated using joint paired residual circular moving-block bootstrap resampling. The same five-year calendar-block indices are applied to contemporaneous MAM and OND residual vectors to preserve cross-season dependence (10,000 replicates).

Panel E: Seasonal trend effect sizes. The four source-era-specific MAM and OND Theil–Sen estimates (mm/decade) are presented with 95% residual CBB confidence intervals. The vertical reference line denotes zero temporal trend. Panel E shows confidence intervals for individual seasonal slopes; it does not itself test the difference between MAM and OND. The paired bootstrap in Panels C–D addresses that separate question. All estimates are source-era-specific. The historical nine-year record is treated as exploratory. No pooled trend, pooled seasonal estimate or formal cross-era significance test was undertaken.

Panel F: Dependence-aware trend summary. The table reports sample size, Theil–Sen slope, 95% residual CBB confidence interval, two-sided HAC p-value, Holm-adjusted p-value within each source era and descriptive coefficient of determination (R^2) for the four independent seasonal models. HAC inference uses a Newey–West estimator with a two-year lag and a t-based reference distribution (df=7 for 1991–1999 and df=23 for 2000–2024). Holm adjustment is applied separately to the MAM and OND tests within each era. R^2 is descriptive and is not used to determine trend significance. Separate one-sided directional tests of increasing rainfall are reported as complementary inference and are not combined with the two-sided tests in Panel F.

For each era independently:

$$D_t = MAM_t - OND_t$$

- H_0: The temporal trend in the paired annual MAM–OND rainfall contrast is zero.
- H_1: The temporal trend in the paired annual MAM–OND rainfall contrast is non-zero.

The primary effect estimate is the Theil–Sen slope of D_t, in mm per decade.

- Positive slope: MAM rainfall is increasing relative to OND.
- Negative slope: OND rainfall is increasing relative to MAM.

3.5.1 Temporal change in the relative contribution of MAM and OND rainfall

Seasonality was assessed through the temporal trend in annual paired differences between March–May (MAM) and October–December (OND) national rainfall accumulation. This approach retained the calendar year as the pairing unit and directly evaluated whether the relative rainfall contribution of the two principal rainy seasons changed over time as shown in Figure 5.

Panels A–B: $\beta_{gap} = Sen(MAM - OND)$

Panels C–D: $\Delta\beta = Sen(MAM) - Sen(OND)$

This manuscript is a preprint and has not been peer reviewed. The copyright holder has made the manuscript available under a Creative Commons Attribution 4.0 International (CC BY) license and consented to have it forwarded to EarthArXiv for public posting.

3.5.2 Seasonal rainfall trends and relative MAM–OND accumulation

A) Individual seasonal rainfall trends

During 1991–1999, both seasons had positive Theil–Sen estimates, although uncertainty was substantial. MAM increased at an estimated 50.84 mm per decade (95% CBB CI: −1.02 to 128.13), while OND increased at 12.95 mm per decade (−106.05 to 152.23). Neither trend was supported by two-sided HAC inference (p=0.125 and p=0.417, respectively; Holm-adjusted p=0.249 and p=0.417). The short historical record therefore provides insufficient evidence of systematic seasonal rainfall increases.

During 2000–2024, MAM exhibited a positive Theil–Sen slope of 28.66 mm per decade (95% CBB CI: 7.55–40.78). Its two-sided HAC test indicated nominal significance before multiplicity adjustment (p=0.0266). The corresponding Holm-adjusted p-value was 0.0532, marginally above the conventional 0.05 threshold. Thus, MAM had a positive bootstrap interval and nominally significant unadjusted HAC evidence, but did not meet the 5% threshold after within-era multiplicity correction. OND also exhibited a positive estimated trend of 14.65 mm per decade, but its 95% CBB confidence interval (−2.28 to 31.03) included zero.

The two-sided HAC test was not significant (p=0.0707; Holm-adjusted p=0.0707). Consequently, the two-sided analysis provides less conclusive evidence of increasing OND rainfall.

B) Directional evidence of increasing seasonal rainfall, 2000–2024

A separate one-sided analysis evaluated the hypothesis of increasing seasonal rainfall accumulation (H_0: $\beta \leq 0$; H_1: $\beta > 0$), using HAC lag and circular block-bootstrap sensitivity analyses. The results summarized in Table 6 are presented alongside the two-sided seasonal trend inference to distinguish evidence of a positive directional trend from evidence based on two-sided testing and within-era multiplicity adjustment.

Table 6: Two-sided and directional evidence of increasing MAM and OND rainfall accumulation in Kenya, 2000–2024

Evidence	MAM	OND
Theil–Sen slope (mm/decade)	+28.66	+14.65
Two-sided residual CBB 95% CI (mm/decade)	+7.55 to +40.78	−2.28 to +31.03
Two-sided HAC p-value (lag 2)	**0.0266**	0.0707
Two-sided HAC p-value, Holm-adjusted	0.0532	0.0707
One-sided HAC p-value (lag 2)	**0.0164**	**0.0411**
One-sided HAC 95% lower confidence bound (mm/decade)	+9.59	+1.61
One-sided bootstrap 95% lower bound (mm/decade)	+17.88	+11.73
Directional robustness classification	Robust	Primary settings only

Abbreviations: CBB, circular residual moving-block bootstrap; HAC, heteroskedasticity- and autocorrelation-consistent inference. The two-sided Holm adjustment applies to the two seasonal tests within the 2000–2024 source era. One-sided results are from a separate directional analysis and are not multiplicity-adjusted in this table.

MAM showed the strongest evidence of an increasing trend. Its positive CBB confidence interval and unadjusted two-sided HAC test (p=0.0266) supported an increase, although the Holm-adjusted p-value (0.0532) narrowly exceeded the 0.05 threshold. The separate one-sided analysis provided additional directional support (p=0.0164), with positive lower confidence bounds under both HAC and bootstrap inference. This support persisted across all tested HAC lags (1, 2 and 3 years) and bootstrap block lengths (3, 5 and 7 years), supporting classification as a robust increase under the specified sensitivity criteria.

OND also had a positive estimated trend, but its two-sided CBB confidence interval included zero and its HAC test was not significant (p=0.0707). Although the one-sided analysis supported an increase under the primary settings (p=0.0411), the result was not consistent across all sensitivity settings. In particular, directional support varied with HAC lag and therefore did not meet the full robustness criterion.

This manuscript is a preprint and has not been peer reviewed. The copyright holder has made the manuscript available under a Creative Commons Attribution 4.0 International (CC BY) license and consented to have it forwarded to EarthArXiv for public posting.

Neither season demonstrated robust directional evidence of increasing rainfall during the shorter 1991–1999 historical period. Overall, the directional analysis reinforces the stronger evidence of increasing MAM rainfall during 2000–2024, while indicating less consistent support for OND. These findings complement the paired inter-seasonal results, which did not establish a statistically distinguishable difference between the MAM and OND trend rates or a temporal change in their signed annual rainfall accumulation gap. The increasing direction should be interpreted as confirmatory only if it was specified independently of the observed trend estimates; otherwise, the one-sided results provide complementary exploratory evidence.

C) Paired comparison of seasonal trend rates

The difference between the independently estimated seasonal Sen slopes was positive in both source eras: +37.89 mm per decade during 1991–1999 and +14.01 mm per decade during 2000–2024. However, the corresponding joint paired residual bootstrap 95% confidence intervals included zero (−101.39 to 160.05 and −8.52 to 31.01 mm per decade, respectively). Thus, neither era provided sufficient evidence that the MAM and OND trend rates differed statistically.

D) Temporal change in the annual MAM–OND accumulation gap

The signed annual MAM-minus-OND contrast provided a second, distinct assessment of relative seasonal rainfall accumulation. During 1991–1999, its Theil–Sen slope was +47.35 mm per decade (95% CBB CI: −85.56 to 210.09). HAC regression produced a slope of −14.63 mm per decade (95% CI: −206.41 to 177.15; p=0.862). During 2000–2024, the signed annual gap had a Theil–Sen slope of +7.75 mm per decade (95% CBB CI: −20.22 to 32.25). HAC regression estimated a slope of +10.83 mm per decade (95% CI: −25.48 to 47.14; p=0.543). Neither source era provided statistically supported evidence of a temporal trend in the annual additive MAM–OND rainfall difference.

3.5.3 Season-specific P20 rainfall deficits

Season-specific P20 rainfall deficits were assessed independently for the two source periods, 1991–1999 and 2000–2024, as summarised in Figure 6.

A) Season-specific P20 rainfall deficit results

Tables 7 and 8 present the season-specific P20 deficit frequencies and the joint occurrence of seasonal deficits across the two source periods.

Table 7: Season-specific P20 rainfall deficit details

Source era	Season	P20 threshold (mm)	Deficit years (n/N)	Specific deficit years	Observed probability	Paired-year CBB 95% CI
1991–1999	MAM	226.19	2/9	1992, 1993	22.22%	0–44.44%
1991–1999	OND	138.89	2/9	1996, 1998	22.22%	0–44.44%
2000–2024	MAM	190.44	5/25	2000, 2009, 2011, 2019, 2022	20.00%	8–32%
2000–2024	OND	175.14	5/25	2005, 2007, 2008, 2010, 2016	20.00%	4–40%

Notes: P20 denotes the season-specific empirical 20th-percentile rainfall threshold, calculated independently for each season and source era using linear quantile interpolation. A deficit year is one in which seasonal rainfall was strictly below its respective P20 threshold. CBB denotes circular moving-block bootstrap. Confidence intervals are conditional on the estimated thresholds; threshold-estimation uncertainty was not propagated.

This manuscript is a preprint and has not been peer reviewed. The copyright holder has made the manuscript available under a Creative Commons Attribution 4.0 International (CC BY) license and consented to have it forwarded to EarthArXiv for public posting.

Table 8: Joint seasonal P20 occurrence results

Source era	MAM-only deficit	OND-only deficit	Both seasons deficit	Neither season deficit
1991–1999	2/9 (22.22%)	2/9 (22.22%)	0/9 (0%)	5/9 (55.56%)
2000–2024	5/25 (20.00%)	5/25 (20.00%)	0/25 (0%)	15/25 (60.00%)

Figure 6 presents the source-era-specific analyses of MAM and OND seasonal rainfall accumulation and lower-tail deficit occurrence. Annual seasonal totals and Theil–Sen trends are shown alongside complementary one-sided HAC tests of directional increases, while the lower panels summarise season-specific empirical P20 deficit frequencies and paired-year circular block-bootstrap confidence intervals. The two periods (1991–1999 and 2000–2024) are analysed independently, allowing seasonal trend behaviour and deficit occurrence to be assessed without pooling the source records.

B) Season-specific P20 rainfall deficit probabilities

The season-specific P20 analysis provided a complementary description of rainfall deficit frequency. During 1991–1999, the MAM P20 threshold was 226.19 mm and the OND threshold was 138.89 mm. Each season recorded two deficit years among the nine available years, corresponding to empirical probabilities of 22.22%. The paired-year CBB 95% intervals were 0–44.44% for both seasons, reflecting the substantial uncertainty associated with the short historical record.

During 2000–2024, the MAM P20 threshold was 190.44 mm, while the OND threshold was 175.14 mm. Each season recorded five deficit years among 25 observations, producing an empirical deficit probability of 20.00%. The paired-year CBB interval was 8–32% for MAM and 4–40% for OND. The wider OND interval indicates greater uncertainty around its estimated deficit probability.

The similar empirical probabilities across MAM and OND during 2000–2024 indicate that neither season had a higher observed frequency of season-specific P20 deficits in this analysis. However, the thresholds were estimated separately for each source era and season. Consequently, these probabilities describe within-era seasonal deficit frequency rather than change in absolute rainfall-deficit risk between historical and recent periods. The analysis also does not propagate uncertainty in estimation of the P20 thresholds into the reported probability intervals.

C) Joint occurrence and non-occurrence of seasonal rainfall deficits

No calendar year in either source era experienced simultaneous MAM and OND rainfall deficits below their respective P20 thresholds. The deficit events occurred in different years, with neither-season deficit conditions recorded in five of nine years (55.6%) during 1991–1999 and 15 of 25 years (60.0%) during 2000–2024. Thus, most observed years in both periods had neither rainy season falling below its season-specific P20 threshold. These complementary frequencies indicate the absence of concurrent lower-tail rainfall events in the paired annual records, although they do not establish the absence of other forms of drought or within-season rainfall deficits.

4. Discussion

4.1 Annual wetting and the contrasting evidence from seasonal rainfall

The national annual rainfall analysis indicates a statistically supported upward trend in Kenya's CHIRPS rainfall series over 2000–2024. The Theil–Sen slope was +78.25 mm per decade (95% circular block-bootstrap confidence interval [CI]: 43.74–102.91), while the complementary Newey–West heteroskedasticity and autocorrelation-consistent (HAC) estimate was +80.86 mm per decade (95% CI: 20.96–140.76; p = 0.0103).

This manuscript is a preprint and has not been peer reviewed. The copyright holder has made the manuscript available under a Creative Commons Attribution 4.0 International (CC BY) license and consented to have it forwarded to EarthArXiv for public posting.

The direction of the annual trend was retained across the tested block-bootstrap lengths and HAC lag specifications. This result establishes an upward national annual rainfall tendency over the period examined, but its interpretation needs to account for the considerable interannual variation in the series. Annual rainfall averaged 640.08 mm, with a standard deviation of 129.42 mm. Three of the 25 years (12%) were at or below the empirical P10 threshold, and five (20%) were at or below P20.

The seasonal analysis provides an additional level of interpretation. During 2000–2024, the estimated MAM Theil–Sen slope was +28.66 mm per decade, with a 95% circular block-bootstrap interval of +7.55 to +40.78 mm per decade. Its two-sided HAC test produced a nominal p-value of 0.0266; however, the within-era Holm-adjusted value was 0.0532. The evidence therefore falls just short of the conventional 0.05 threshold after multiplicity adjustment. A separately conducted one-sided analysis also supported a positive MAM trend ($p = 0.0164$), with positive lower confidence bounds across the tested HAC lag and bootstrap block-length specifications. That directional result strengthens the evidence for an increase.

OND also had a positive estimated trend, with a Theil–Sen slope of +14.65 mm per decade. However, its 95% circular block-bootstrap interval extended from −2.28 to +31.03 mm per decade. The corresponding two-sided HAC estimate was +28.21 mm per decade (95% CI: −2.58 to +59.01; $p = 0.0707$). A separate one-sided test produced $p = 0.0411$, but its positive lower bounds were retained only under the primary settings, rather than across the full sensitivity analysis. The OND result was consequently interpreted as a positive but less robust indication of increasing seasonal accumulation, not as equivalent in strength to the MAM evidence.

This distinction matters for the interpretation of the two rainy seasons. Both had positive point estimates during 2000–2024, but the evidence supporting an increase was stronger for MAM. The paired analysis did not, however, establish that MAM rainfall increased faster than OND rainfall. The estimated difference between their seasonal Sen slopes was +14.01 mm per decade, with a paired circular block-bootstrap 95% CI of −8.52 to +31.01 mm per decade. Because this interval includes zero, the observed difference in point estimates does not establish a statistically distinguishable difference in the rates of seasonal change.

The separate analysis of the annual MAM–OND rainfall gap leads to the same restraint in interpretation. The Sen slope for the annual signed difference, defined as MAM minus OND rainfall, was +7.75 mm per decade (95% CI: −20.22 to +32.25). The corresponding HAC coefficient was +10.83 mm per decade (95% CI: −25.48 to +47.14; $p = 0.543$). Thus, there was no statistically supported temporal change in the annual difference between the two seasonal totals. This analysis addresses a different estimand from the paired difference between the two individual seasonal Sen slopes: the trend in the annual MAM–OND gap is not interchangeable with the difference between the two estimated seasonal trends. Neither analysis provides evidence that the two seasons have become progressively more divergent.

The short 1991–1999 historical record provides limited additional context. The estimated MAM and OND Sen slopes were +50.84 and +12.95 mm per decade, respectively, but their confidence intervals were broad and included zero. The paired difference between the seasonal slopes was also imprecise, with a 95% interval of −101.39 to +160.05 mm per decade. The trend in the annual MAM–OND gap was not established either: its Sen estimate was +47.35 mm per decade (95% CI: −85.56 to +210.09), while the HAC estimate was −14.63 mm per decade ($p = 0.862$).

With only nine annual observations, these historical estimates are exploratory and are not given the same inferential weight as the 25-year CHIRPS analysis. In addition, the historical series was supplied as a national tabular dataset whose upstream grid provenance and aggregation procedure could not be verified; it was not homogenised with CHIRPS. The two periods therefore were not treated as a single continuous record from which a formal change in rainfall trend can be inferred.

This manuscript is a preprint and has not been peer reviewed. The copyright holder has made the manuscript available under a Creative Commons Attribution 4.0 International (CC BY) license and consented to have it forwarded to EarthArXiv for public posting.

The annual and seasonal findings are consequently consistent in showing positive rainfall tendencies in the recent period, but they do not establish a uniform or seasonally divergent response. The annual estimate concerns rainfall accumulated across the calendar year, while MAM and OND represent only two components of that total. The annual increase cannot be attributed entirely to either rainy season without examining the other months and the contribution of rainfall outside the two main seasons. Moreover, the seasonal results indicate that positive accumulation trends can coexist with individual years of relatively low seasonal rainfall.

4.2 Convergence with evidence of seasonal and spatial rainfall variability in eastern Africa

The combined findings are consistent with the broader evidence that eastern African rainfall is characterised by distinct seasonal regimes, multiple climatic controls and substantial spatial variation. Nicholson's regional synthesis describes the differences in rainfall seasonality and variability across eastern Africa, including the distinct relationships between the long and short rains and their respective climate drivers [1]. Palmer and colleagues similarly identify the influence of the El Niño–Southern Oscillation and Indian Ocean Dipole on interannual rainfall variability, while emphasising that observed trends differ between seasons and have varied over time [2].

The seasonal context in Palmer et al. is particularly relevant. Their synthesis describes a tendency towards declining long-rains rainfall from the mid-1980s to around 2010, followed by partial recovery in some areas, while the short rains generally became wetter over much of eastern Africa. The present analysis, which covers 2000–2024, identifies a positive MAM accumulation trend and a positive but less statistically secure OND trend. The MAM result is therefore compatible with the reported partial recovery in the more recent part of the regional record, although the two analyses differ in spatial coverage, data treatment and period of inference. The positive OND estimate is also consistent with the broader regional evidence of increasing short-rains accumulation, but the present result does not establish an equally robust increase for Kenya at the national scale [2].

Research using higher-resolution rainfall datasets further supports the need to distinguish regional and national patterns from local rainfall behaviour. Gebrechorkos et al. reported spatially differentiated rainfall trends across Ethiopia, Kenya and Tanzania, including decreasing long-rains rainfall in eastern parts of the region and contrasting changes elsewhere. Their short-rains analysis identified generally non-significant increases across large parts of the region [17]. Similarly, Kotikot et al. found both wetting and drying patterns across Kenyan counties during the long and short rains, alongside evidence of increased seasonal and intraseasonal variability and more frequent extreme wet and dry events [5]. These studies demonstrate that a positive national seasonal or annual estimate does not necessarily represent a consistent response across counties.

The present findings add to this literature by bringing together national annual rainfall trends, separate MAM and OND trend estimates, paired seasonal comparisons and the joint occurrence of lower-tail seasonal years. This combination helps distinguish three features that may otherwise be conflated: the direction of annual rainfall change, the strength of evidence for seasonal changes, and the extent to which low-rainfall conditions occur in both seasons during the same year. The findings suggest that the recent national annual increase occurred alongside positive seasonal estimates, but without statistical evidence that the two rainy seasons followed different rates of change. At the same time, the continued occurrence of seasonal lower-tail years shows that a positive accumulation trend does not remove year-to-year rainfall deficits.

The convergence with regional evidence is therefore not that all studies demonstrate the same direction of rainfall change. It is that rainfall change is strongly dependent on the season, geographical domain, observation period and indicator used. The present national annual and seasonal results should be interpreted within that framework, rather than as a replacement for county-level or sub-seasonal assessments.

This manuscript is a preprint and has not been peer reviewed. The copyright holder has made the manuscript available under a Creative Commons Attribution 4.0 International (CC BY) license and consented to have it forwarded to EarthArXiv for public posting.

4.3 Divergence from reported long-rains drying and the importance of the observation period

The positive MAM estimate in the present analysis differs in direction from studies that documented long-rains drying across parts of eastern Africa during earlier periods. Wainwright et al. described a decline in the eastern African long rains associated with later onset and earlier cessation, rather than a comparable reduction in peak area-averaged daily rainfall intensity. Their analysis also identified partial recovery in the more recent years of their observation period [3]. Palmer et al. likewise describes the long-rains drying tendency that persisted from the mid-1980s to around 2010, followed by some recovery thereafter [2].

The difference in period is important. The present MAM analysis covers 2000–2024 and therefore includes years within the previously reported drying period as well as the subsequent period of partial recovery. Its positive trend should not be interpreted as evidence that the earlier long-rains drying observations were incorrect. Rather, it represents the net direction of the national seasonal rainfall series over a later and differently defined period. It is possible for a trend estimated across 2000–2024 to be positive even when part of that period experienced lower rainfall, particularly where later recovery contributes to the overall slope. The current analysis does not, however, identify the timing or mechanism of any such change.

Cattani et al. provide a further reason for caution when comparing seasonal trends. Their analysis of ARC2, CHIRPS and TAMSAT rainfall products for 1983–2015 found that trend patterns varied by product, geographical area and rainfall indicator. Their results included indications of declining MAM rainfall over substantial parts of eastern Africa, but the spatial distribution and statistical support were not consistent across the three satellite products. Their analysis also identified increases in several OND indicators over eastern Africa, with Kenya an exception to the broader regional pattern [4]. The present results do not resolve these earlier product and spatial differences. They provide a later national estimate derived from the specified CHIRPS series, rather than a county-resolved comparison among satellite products.

The difference between annual and seasonal findings also has an important statistical explanation. Annual rainfall represents the accumulated rainfall from all months of the year. A positive annual trend can therefore arise from changes in MAM, OND, other rainfall periods, or a combination of them. It can also coexist with changes in the timing and distribution of rainfall within a season.

An increase in a seasonal total does not necessarily indicate that rainfall is spread more evenly across the season, that the season starts earlier, or that it lasts longer. Wainwright et al.'s finding that the long-rains decline was associated with later onset and earlier cessation, rather than a comparable decline in peak daily rainfall, illustrates how seasonal accumulation can change through altered rainfall timing [3].

The 2024 Kenya climate assessment provides a recent illustration of why national and seasonal rainfall indicators need to be interpreted together. The Kenya Meteorological Department reported substantial spatial variation during 2024, with above-normal MAM rainfall in parts of the western and central highlands, but near- or below-normal conditions in other areas. The report also documented below-average OND rainfall and deteriorating drought and food-security conditions in affected areas [18]. These observations illustrate the practical consequences of seasonal and geographical contrasts, but do not independently validate the long-term trend estimated here.

It is also important not to equate the Kenya Meteorological Department's classification of a season as below average with the present study's P20 deficit classification. The two classifications use different thresholds and may be based on different spatial and temporal aggregations. A season can be below its climatological average without falling below the empirical twentieth percentile used in this analysis. This distinction is particularly important when comparing the 2024 assessment with the present annual and seasonal classifications. Taken together, the apparent divergence from earlier reports of long-rains drying is best understood in terms of differences in observation period, spatial coverage and rainfall metric.

This manuscript is a preprint and has not been peer reviewed. The copyright holder has made the manuscript available under a Creative Commons Attribution 4.0 International (CC BY) license and consented to have it forwarded to EarthArXiv for public posting.

The positive MAM trend during 2000–2024 is evidence of increasing national seasonal accumulation over that interval. It does not establish a long-term reversal of all previously documented drying patterns, nor does it demonstrate that the timing, duration or reliability of MAM rainfall has recovered uniformly across Kenya.

4.4 Seasonal deficit occurrence and the absence of concurrent MAM–OND lower-tail years

The P20 analysis adds a dimension that is not captured by trend estimates alone. During 2000–2024, five MAM years and five OND years fell strictly below their respective season-specific P20 thresholds. These were not the same years. The MAM deficit years were 2000, 2009, 2011, 2019 and 2022, while the OND deficit years were 2005, 2007, 2008, 2010 and 2016. No calendar year was classified as a deficit year in both seasons. Consequently, 10 of the 25 years (40%) experienced a lower-tail deficit in one season only, while 15 years (60%) had neither MAM nor OND rainfall below its corresponding P20 threshold.

The historical series showed the same pattern of non-concurrent seasonal deficits. MAM fell below its P20 threshold in 1992 and 1993, while OND fell below its threshold in 1996 and 1998. Again, no year had both seasons below their respective thresholds. Five of the nine years (55.6%) had neither a MAM nor an OND deficit.

These results show that the observed lower-tail MAM and OND events were seasonally non-concurrent within the annual records examined. In the recent period, most years did not fall below either season's own P20 threshold, despite the continued occurrence of lower-tail years in both seasons. This is compatible with the positive seasonal accumulation estimates: an overall upward tendency does not preclude individual years with relatively low seasonal totals.

The joint classification also provides an important qualification to the marginal P20 frequencies. The five MAM deficit years and five OND deficit years during 2000–2024 each represent 20% of their respective annual series. Because the thresholds were estimated from the same period's observations, these marginal frequencies describe the empirical lower tails of the selected series; they should not be interpreted as independent estimates of future drought probability. The absence of a year classified below P20 in both seasons is a feature of the observed paired annual classifications. It does not establish statistical independence between MAM and OND rainfall, nor does it demonstrate that Kenya was free from drought in years classified as having neither seasonal P20 deficit.

In particular, neither-season classification should not be equated with an absence of agricultural, hydrological or socioeconomic drought. A seasonal total can remain above its P20 threshold while containing prolonged dry spells, delayed onset, early cessation or an uneven distribution of rainfall. Similarly, rainfall deficits at county or sub-county scales may not be reflected in the national seasonal total. The observed joint states therefore describe the concurrence of two specific national seasonal lower-tail indicators, rather than the full range of drought conditions at sub-national levels.

The historical and recent state distributions are descriptively similar in that neither period recorded simultaneous MAM and OND P20 deficits. However, the small historical sample and the differences in source data preclude a strong comparative claim about changes in the probability of concurrent seasonal deficits. Overall, we concluded that no concurrent lower-tail MAM–OND year was observed in either era-aware source period.

4.5 Measurement and inferential considerations

The results depend on both the characteristics of the rainfall product and the spatial and temporal aggregation used in the analysis. CHIRPS is widely used for rainfall monitoring over eastern Africa, and its evaluation against gauge observations supports its utility at regional scales. However, Dinku et al. found that product performance varies geographically, with weaker performance in some coastal and mountainous settings [7]. This is relevant to Kenya, where terrain, coastal influences and pronounced rainfall gradients can affect the representation of precipitation in gridded products.

This manuscript is a preprint and has not been peer reviewed. The copyright holder has made the manuscript available under a Creative Commons Attribution 4.0 International (CC BY) license and consented to have it forwarded to EarthArXiv for public posting.

National aggregation also reduces the visibility of local differences. It provides a useful summary of country-level rainfall accumulation, but it does not describe the distribution of rainfall among counties or identify the locations where rainfall changed most strongly. A positive national trend may therefore coexist with declining rainfall in some areas, just as a positive seasonal trend may coexist with county-level seasonal deficits. The findings should be interpreted as national estimates from the supplied CHIRPS series, not as evidence of equivalent rainfall changes throughout the country.

The length of the CHIRPS record also constrains inference. Twenty-five annual observations provide a basis for estimating the trend, but remain a relatively short sample for characterising low-frequency rainfall variability. HAC and circular block-bootstrap procedures address specified forms of temporal dependence, and the sensitivity analyses provide some assurance that the main annual result is not dependent on a single lag or block-length choice. They cannot, however, eliminate uncertainty associated with a short record, possible non-stationarity or errors in the underlying rainfall estimates.

The seasonal analyses introduce further inferential distinctions. The seasonal Sen estimates, HAC regression coefficients and paired bootstrap intervals are not interchangeable statistics. Theil–Sen estimates the median pairwise slope, while the HAC model estimates a linear regression coefficient with a covariance adjustment for heteroskedasticity and autocorrelation. Their numerical differences do not necessarily indicate inconsistency. Similarly, the paired difference between MAM and OND Sen slopes answers a different question from the trend in the annual signed MAM–OND gap. Keeping these estimands distinct is essential when interpreting whether the two seasons have changed at different rates.

The P20 analysis is also conditional on the thresholds estimated from the respective annual series. Its paired-year confidence intervals do not propagate the uncertainty arising from estimation of the P20 thresholds themselves. The historical period, with only nine years, is especially sensitive to the small number of observations. Its deficit frequencies and joint states should be treated as descriptive rather than as stable estimates of the long-term occurrence of seasonal rainfall extremes.

4.6 Implications for drought monitoring, population exposure and climate–health vulnerability assessment

The combined annual, seasonal and joint-deficit findings have direct implications for the way rainfall information is used in climate-risk monitoring. The positive annual trend should not, by itself, be used to infer that drought preparedness can be reduced. Annual accumulation is only one dimension of rainfall exposure. The seasonal results show that MAM and OND require separate interpretation, while the P20 classifications demonstrate that lower-tail seasonal years continued to occur despite positive trend estimates. For agriculture and food security, seasonal rainfall totals need to be interpreted alongside the timing and distribution of rainfall during crop and pasture development. A season with a positive long-term accumulation trend may still contain years with low total rainfall, delayed onset, early cessation or extended dry spells. These characteristics can affect planting decisions, crop development and pasture availability, but were not directly measured in the present analysis. The findings therefore support retaining season-specific indicators rather than relying on annual rainfall trends as a proxy for agricultural water availability. The same distinction applies to water resources. Annual rainfall accumulation alone cannot establish changes in soil moisture, groundwater recharge, streamflow, reservoir inflow or the duration of water shortages. These outcomes depend on rainfall intensity and distribution, evapotranspiration, catchment characteristics, land cover and water-management practices. The present analysis provides a national precipitation signal and a description of selected lower-tail conditions; it does not quantify changes in hydrological drought or water security.

For climate-health assessment, rainfall is an important hazard-related variable, but the annual and seasonal estimates reported here do not constitute evidence of changing disease incidence or health outcomes. Heavy rainfall and flooding can affect water quality, sanitation and access to health services, while rainfall deficits can place pressure on domestic water supplies, food security and livelihoods.

This manuscript is a preprint and has not been peer reviewed. The copyright holder has made the manuscript available under a Creative Commons Attribution 4.0 International (CC BY) license and consented to have it forwarded to EarthArXiv for public posting.

The consequences depend on where rainfall occurs, when it occurs, the intensity and duration of the event, and the population's exposure and adaptive capacity. The 2024 Kenya climate assessment illustrates how contrasting seasonal conditions can produce flooding and drought-related pressures within the same year [18].

Health implications therefore require integration of rainfall indicators with relevant environmental, epidemiological, health-service and vulnerability data. These findings also have implications for population-based climate–health vulnerability assessment. Seasonal rainfall should be treated as a time-varying hazard indicator rather than a direct measure of population health risk. Climate-related risk arises through the interaction of hazards with the location of exposed populations and their sensitivity and adaptive capacity [19]. Consequently, nationally aggregated annual or seasonal rainfall estimates cannot establish how many people are exposed, where exposure is concentrated, or which populations may have limited capacity to cope. Separate season-aware (MAM and OND) hazard assessments should therefore be spatially aligned with population distributions to estimate the number and proportion of people within season-specific climate-hazard zones.

These exposure estimates can then be integrated with indicators of population sensitivity and adaptive capacity, including water and sanitation access, food security, livelihoods and health-service capacity. This would help distinguish seasonal hazard patterns from their geographically differentiated population and health-system implications [20,21].

A more complete monitoring framework should combine season-specific rainfall indicators with spatially resolved hazard assessments and gridded or census-based population data. Population counts and proportions within seasonal hazard zones should be estimated at sub-national and, where data permit, sub-county resolution. Rainfall indicators should therefore extend beyond annual to seasonal accumulation, and where stable datasets exist to include onset and cessation, wet-day frequency, consecutive dry days, rainfall intensity and precipitation indices at appropriate accumulation periods. These indicators should be interpreted alongside soil moisture, evaporative demand, streamflow, groundwater and crop-condition measures. Integration with population sensitivity, epidemiological surveillance and health-service coverage would provide a stronger basis for identifying geographically differentiated climate–health vulnerabilities and targeting seasonal preparedness. Such an approach would also help distinguish meteorological rainfall variability from agricultural, hydrological and socioeconomic drought. This paper's findings was conceptually translated into recommended next step as shown in figure 7.

4.7 Limitations

Several limitations qualify the interpretation of these findings. First, the current CHIRPS annual analysis covers 2000–2024 and contains only 25 observations covering the Kenya county regimes. Although the dependence-aware methods and sensitivity analyses support the reported annual trend, the record cannot fully characterise longer-term variability or establish whether the trend will persist. Second, the 1991–1999 historical series was obtained as a national tabular dataset whose upstream grid provenance and aggregation procedure could not be verified; it was not homogenised with CHIRPS. Though almost all era-aware inferences are consistent through the 1991-2024 window, the 1991-1999 era was treated as a separate exploratory period and was not pooled with the recent series for inferential trend estimation. It however provided us with opportunity to appreciate possible inferential differences based on source datasets and spatial resolution differences [4]. Third, the annual analysis is national in scale. It does not resolve county-level differences in rainfall accumulation or localized lower-tail conditions. Fourth, the seasonal totals do not capture rainfall onset, cessation, intraseasonal distribution, wet-day frequency, intensity or consecutive dry periods.

The observed positive seasonal trends should not be interpreted as evidence of improved seasonal reliability. Fifth, the empirical P10 and P20 thresholds are relative to the observed series, rather than externally calibrated thresholds like SPI-3 for agricultural or hydrological drought. The P20 joint-state estimates are conditional on these thresholds and do not account for their estimation uncertainty.

This manuscript is a preprint and has not been peer reviewed. The copyright holder has made the manuscript available under a Creative Commons Attribution 4.0 International (CC BY) license and consented to have it forwarded to EarthArXiv for public posting.

Finally, satellite rainfall estimates have spatially varying performance, particularly in coastal and mountainous areas [7]. The findings are consequently conditional on the selected CHIRPS product and national aggregation. Independent gauge-based assessment, comparison with other long-term rainfall products, and county-resolved analyses would strengthen the interpretation of spatial trends and lower-tail conditions. These limitations do not negate the observed national annual increase, but they define the scope of the conclusions that can be drawn from it.

5. Conclusion

National annual rainfall in Kenya showed an upward trend during the 2000–2024 CHIRPS period, but the seasonal analysis demonstrated that the evidence was not uniform across the two principal rainy seasons. Both MAM and OND had positive estimated trends, with stronger evidence supporting an increase in MAM. However, the paired analyses did not establish a statistically distinguishable difference between their trend rates or a temporal change in the annual MAM–OND rainfall accumulation gap.

Season-specific lower-tail rainfall years continued to occur in both rainy seasons. However, no calendar year in either source period recorded simultaneous MAM and OND rainfall below their respective P20 thresholds. These classifications describe relative seasonal rainfall deficits within the observed distributions and do not establish the absence of other forms of drought. The 1991–1999 historical series remains exploratory and is interpreted separately from the CHIRPS period.

For climate-risk monitoring, national annual rainfall trends should therefore be considered alongside separate MAM and OND indicators, seasonal deficit occurrence and spatially resolved rainfall patterns. Further assessment incorporating rainfall onset and cessation, dry-spell duration, intensity, hydrological conditions and population exposure is necessary before drawing conclusions about agricultural drought, water security or climate-related health risks.

Funding: The authors received no specific financial support for this study.

Competing interests: The authors declare that they have no competing interests.

Author contributions: Solomon M. Nzioka conceived the study, led the methodology, computing and evidence curation, and coordinated manuscript development. Bosco L. Lolem contributed primary data review. Emmanuel Wamalwa contributed epidemiological and statistical review. Jeremiah Mushosho contributed data-quality and risk-management review. All authors reviewed and approved the manuscript.

Data availability: CHIRPS version 2.0 precipitation data for 2000–2024 are publicly available from the Climate Hazards Center [8]. The historical Kenya rainfall dataset (1991–2016), from which the 1991–1999 national reference was subset, is publicly catalogued by Code for Africa on openAFRICA and attributed there to the World Bank Climate Change Knowledge Portal [9]. Supplementary Table S1 summarises the source provenance, spatial support and resolution information, including the limits of the historical source metadata. The derived rainfall datasets, analysis scripts, machine-readable statistical results, data dictionaries, provenance documentation and quality-assurance manifests supporting this study are available from Zenodo: https://zenodo.org/records/23951555 [22]. The deposit documents the separate 1991–1999 historical and 2000–2024 CHIRPS analytical periods. It includes derived national monthly rainfall inputs but does not include the complete original CHIRPS GeoTIFF archive or the upstream raster-to-national aggregation workflow.

This manuscript is a preprint and has not been peer reviewed. The copyright holder has made the manuscript available under a Creative Commons Attribution 4.0 International (CC BY) license and consented to have it forwarded to EarthArXiv for public posting.

References

1. Nicholson SE. Climate and climatic variability of rainfall over eastern Africa. Reviews of Geophysics. 2017;55(3):590–635. doi:10.1002/2016RG000544.
2. Palmer PI, Wainwright CM, Dong B, Maidment RI, Wheeler KG, Gedney N, et al. Drivers and impacts of Eastern African rainfall variability. Nature Reviews Earth & Environment. 2023;4(4):254–270. doi:10.1038/s43017-023-00397-x.
3. Wainwright CM, Marsham JH, Keane RJ, Finney DL, Black E, Rowell DP, et al. "Eastern African Paradox" rainfall decline due to shorter not less intense Long Rains. npj Climate and Atmospheric Science. 2019;2:34. doi:10.1038/s41612-019-0091-7.
4. Cattani E, Merino A, Guijarro JA, Levizzani V. East Africa rainfall trends and variability 1983–2015 using three long-term satellite products. Remote Sensing. 2018;10(6):931. doi:10.3390/rs10060931.
5. Kotikot SM, Smithwick EAH, Greatrex H. Observations of enhanced rainfall variability in Kenya, East Africa. Scientific Reports. 2024;14:12915. doi:10.1038/s41598-024-63786-2.
6. Funk C, Peterson P, Landsfeld M, Pedreros D, Verdin J, Shukla S, et al. The climate hazards infrared precipitation with stations—a new environmental record for monitoring extremes. Scientific Data. 2015;2:150066. doi:10.1038/sdata.2015.66.
7. Dinku T, Funk C, Peterson P, Maidment R, Tadesse T, Gadain H, et al. Validation of the CHIRPS satellite rainfall estimates over eastern Africa. Quarterly Journal of the Royal Meteorological Society. 2018;144(S1):292–312. doi:10.1002/qj.3244.
8. Climate Hazards Center. CHIRPS: Rainfall estimates from rain gauge and satellite observations [Internet]. Santa Barbara (CA): University of California, Santa Barbara; cited 2026 Nov 4. Available from: https://chc.ucsb.edu/data/chirps/.
9. Code for Africa. Kenya Climate Data (1991–2016) – Rainfall(MM) [dataset]. openAFRICA; created 2020 Nov 30; last updated 2020 Nov 30. Resource ID: 25acacc5-c606-4958-9c8a-1b7d6b12d66d. Available from: https://open.africa/dataset/kenya-climate-data-1991-2016/resource/25acacc5-c606-4958-9c8a-1b7d6b12d66d.
10. World Bank. Climate Change Knowledge Portal: Observed Climate Data, CRU TS 4.07 0.5-degree dataset [dataset metadata]. Washington (DC): World Bank; metadata last updated 2024 Jan 31. Available from: https://datacatalog.worldbank.org/infrastructure-data/search/dataset/0040276/climate-change-knowledge-portal-observed-climate-data-cru-ts4-07-0-5-degree.
11. Theil H. A rank-invariant method of linear and polynomial regression analysis. Proceedings of the Koninklijke Nederlandse Akademie van Wetenschappen. 1950;53:386–392, 521–525, 1397–1412.
12. Sen PK. Estimates of the regression coefficient based on Kendall's tau. Journal of the American Statistical Association. 1968;63(324):1379–1389. doi:10.1080/01621459.1968.10480934.
13. Kendall MG. A new measure of rank correlation. Biometrika. 1938;30(1–2):81–93. doi:10.1093/biomet/30.1-2.81.
14. Künsch HR. The jackknife and the bootstrap for general stationary observations. The Annals of Statistics. 1989;17(3):1217–1241. doi:10.1214/aos/1176347265.
15. Politis DN, Romano JP. A circular block-resampling procedure for stationary data. In: LePage R, Billard L, editors. Exploring the Limits of Bootstrap. New York: John Wiley & Sons; 1992. p. 263–270.
16. Newey WK, West KD. A simple, positive semi-definite, heteroskedasticity and autocorrelation consistent covariance matrix. Econometrica. 1987;55(3):703–708. doi:10.2307/1913610.
17. Gebrechorkos SH, Hülsmann S, Bernhofer C. Long-term trends in rainfall and temperature using high-resolution climate datasets in East Africa. Scientific Reports. 2019;9:11376. https://doi.org/10.1038/s41598-019-47933-8
18. Kenya Meteorological Department. State of the Climate Report (2024). Nairobi: Kenya Meteorological Department; 2025. https://meteo.go.ke/publications/state-of-the-climate-report-2024/
19. IPCC. Climate Change 2022: Impacts, Adaptation and Vulnerability. Contribution of Working Group II to the Sixth Assessment Report of the Intergovernmental Panel on Climate Change. Cambridge: Cambridge University Press; 2022. doi:10.1017/9781009325844.
20. World Health Organization. Climate change and health: vulnerability and adaptation assessment. Geneva: World Health Organization; 2021. ISBN: 978-92-4-003638-3. Available from: https://www.who.int/publications/i/item/9789240036383.
21. Ministry of Health, Kenya. The Kenya Climate Change and Health Strategy 2024–2029. Nairobi: Ministry of Health; 2025. Available from: https://health.go.ke/sites/default/files/2025-10/Kenya%20Climate%20Change%20%26%20health%20Strategy%20SIGNED.pdf.
22. Nzioka SM. Kenya national rainfall and equatorial bimodal seasonal rainfall reproducibility package, 1991–2024 (Version 1.0.0) [dataset]. Zenodo. 2026. https://doi.org/10.5281/zenodo.23951555

SUPPLEMENTARY INFORMATION

S1 Table. Rainfall data provenance, spatial support and resolution in the Kenya analysis

Purpose. This table distinguishes the native spatial support of the primary CHIRPS series from the tabular form of the historical reference and from separate CCKP catalogue metadata. The 0.5° CRU TS specification is not attributed to the historical CSV because the public archive record does not establish that lineage.

Source and period used	Delivered format and spatial support	Resolution and temporal coverage	Provenance, processing and interpretive limits
CHIRPS version 2.0 [8] Primary analysis: January 2000–December 2024 300 monthly records	Native gridded precipitation rasters (GeoTIFF), EPSG:4326. The Kenya working subset is described in the manuscript as 159 × 195 cells. National and county supports were selected using the Kenya national boundary and 47 county polygons.	0.05° × 0.05° nominal grid spacing (approximately 5 km); monthly precipitation values. Annual and MAM/OND seasonal accumulations were derived from monthly values.	The national monthly estimate is the arithmetic mean of valid selected pixels (pixel-count weighted), not area- or population-weighted. Boundary-intersecting cells contribute their full native pixel value; no fractional-area adjustment is used. NoData cells are excluded, not imputed or treated as zero.
Code for Africa openAFRICA, "Kenya Climate Data | 1991–2016" Rainfall(MM) CSV [9]. Study subset: January 1991–December 1999 (108 monthly records; nine annual observations). Resource ID: 25acacc5-c606-4958-9c8a-1b7d6b12d66d. Package ID: 1106e169-24ab-404e-bdbf-42a7e2f77c6c.	CSV national monthly tabular series as used in the analysis. The retained analytical file has no spatial coordinates, grid-cell identifiers or county-level identifiers. It is not a georeferenced raster or county-resolved dataset in the form analysed.	Monthly observations, 1991–2016 in the archive; 1991–1999 used. No native grid spacing or underlying spatial resolution is reported or verified for the CSV.	The openAFRICA record attributes the data to the World Bank Climate Change Knowledge Portal. Catalogue creation and last-update dates are 30 Nov 2020; these are not the original CHRIS retrieval date. This nine-year subset is exploratory and was not homogenised or pooled with CHIRPS.
World Bank CCKP, Observed Climate Data: CRU TS version 4.07 0.5-degree dataset [10]. Contextual catalogue metadata only; not confirmed as the source product of the openAFRICA CSV.	Separate gridded observational climate product. The CCKP catalogue describes interpolation of monthly climate anomalies from weather-station observations and notes that both gridded and spatially aggregated products are available.	0.5° × 0.5° latitude–longitude grid. Catalogue coverage: 1901–2022; monthly, seasonal and annual time series. Metadata last updated 31 Jan 2024.	The CCKP catalogue entry does not demonstrate that the particular openAFRICA CSV is a direct extraction or national aggregation of CRU TS 4.07. Therefore, the 0.5° resolution is contextual metadata and must not be assigned to the historical CSV.

Interpretive notes

- The historical input is national tabular data without retained coordinates or cells; CHIRPS is a georeferenced 0.05° monthly raster series.
- The 0.5° CRU TS 4.07 specification belongs to a separate CCKP catalogue entry and is not evidence of the historical CSV's resolution, exact product version or aggregation procedure.
- The 30 November 2020 date is the openAFRICA catalogue date, not the historical CSV's CHRIS ingestion date.
- The short 1991–1999 historical segment remains exploratory and is not pooled with CHIRPS because the source series were not homogenised.

Source references

[8] Climate Hazards Center. CHIRPS v2 dataset page. https://chc.ucsb.edu/data/chirps/.
[9] Code for Africa. Kenya Climate Data (1991–2016), Rainfall(MM) resource 25acacc5-c606-4958-9c8a-1b7d6b12d66d. https://open.africa/dataset/kenya-climate-data-1991-2016/resource/25acacc5-c606-4958-9c8a-1b7d6b12d66d.
[10] World Bank. CCKP Observed Climate Data: CRU TS 4.07 0.5° dataset metadata. https://datacatalog.worldbank.org/infrastructure-data/search/dataset/0040276/climate-change-knowledge-portal-observed-climate-data-cru-ts4-07-0-5-degree.

Increasing national annual rainfall alongside trends in Kenya's equatorial bimodal rainy seasons and recurrent lower-tail years, 2000–2024: dependence-aware analysis with exploratory 1991–1999 context

Kenya's annual and bimodal seasonal rainfall trends, 1991-2024

Research Article

This manuscript is a preprint and has not been peer reviewed. The copyright holder has made the manuscript available under a Creative Commons Attribution 4.0 International (CC BY) license and consented to have it forwarded to EarthArXiv for public posting.

Solomon M. Nzioka[1]*, Bosco L. Lolem[2], Emmanuel Wamalwa[3], Jeremiah Mushosho[4]

[1] Phoenix Climate and Health Impact Experts, Nairobi, Kenya
[2] Climate Change and Health Unit, Ministry of Health, Nairobi, Kenya
[3] Department of Public Health, Daystar University, Nairobi, Kenya
[4] Climate Change, Health and Environment, WHO Regional Office for Africa, Brazzaville, Republic of the Congo
Corresponding author: Solomon M. Nzioka | solomonmn@climate-health-impacts.net | ORCID: 0009-0004-7915-1270

LIST OF FIGURES

Figure 1: Workflow for calculating empirical annual rainfall P10 and P20 thresholds and classifying annual observations 2

Figure 2: National annual rainfall variability and drought thresholds in Kenya, 1991–2024. 3

Figure 3: Theil–Sen confidence intervals under 3 circular block lengths, Newey–West HAC CI under 3 lag specifications 4

Figure 4: Distribution of annual rainfall observations across the three mutually exclusive empirical lower-tail categories.....4

Figure 5: Source-era-specific seasonal rainfall trends and relative MAM–OND accumulation in Kenya, 1991–2024 5

Figure 6: Season-trends and specific P20 rainfall deficit 6

Figure 7: Conceptual steps from climate intelligence to implementation science 7

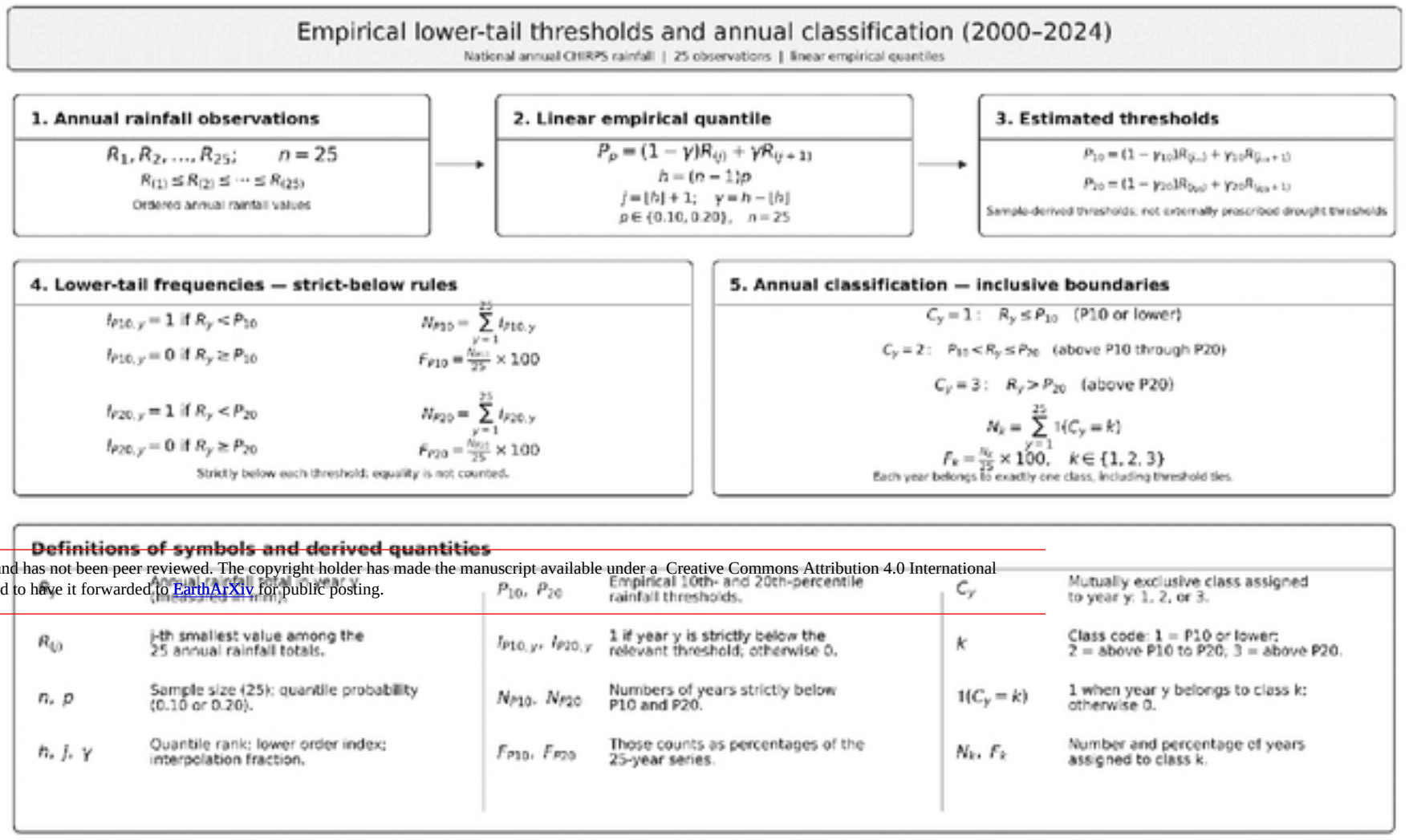
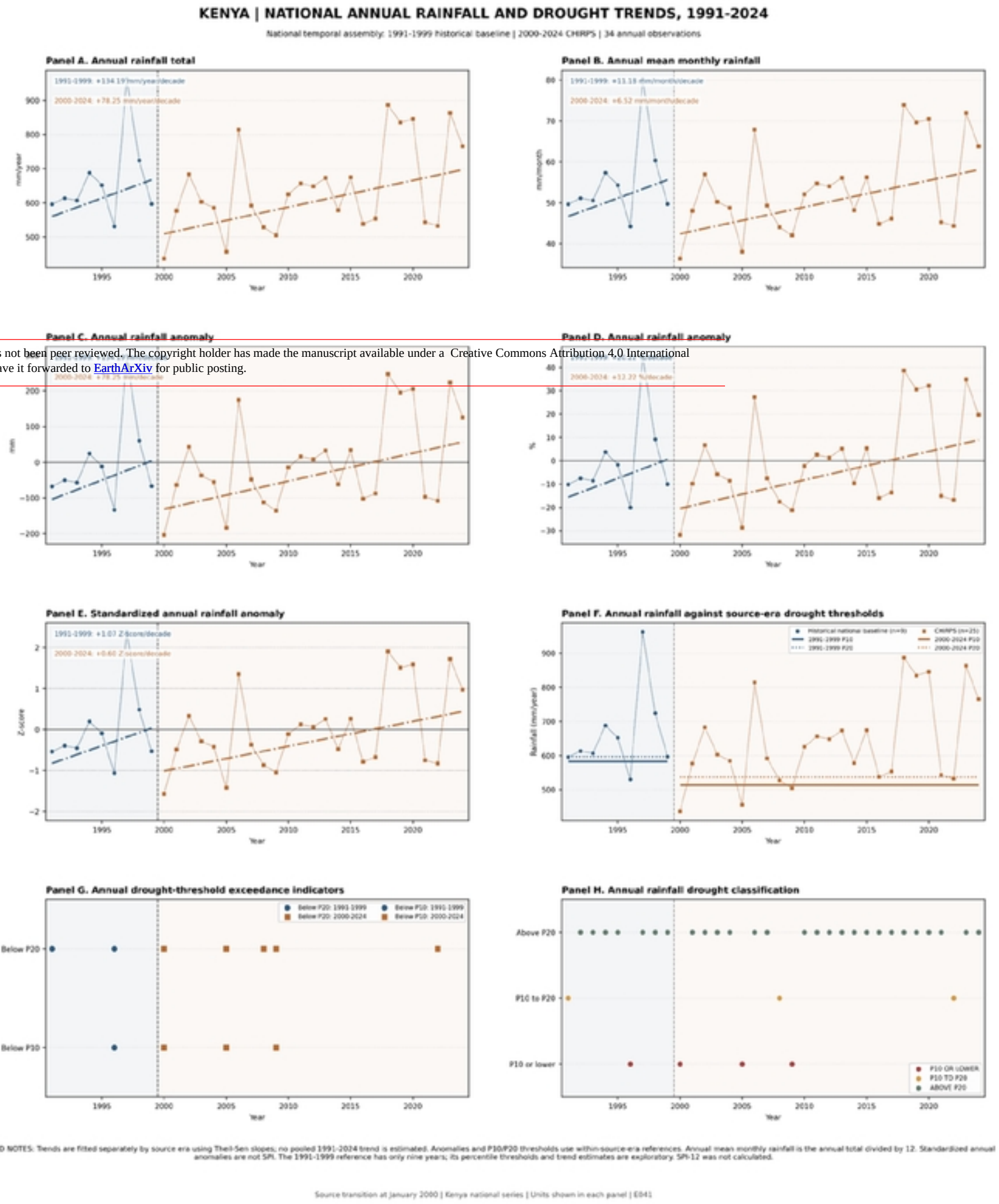


Figure 1: Workflow for calculating empirical annual rainfall P10 and P20 thresholds and classifying annual observations

This manuscript is a preprint and has not been peer reviewed. The copyright holder has made the manuscript available under a Creative Commons Attribution 4.0 International (CC BY) license and consented to have it forwarded to EarthArXiv for public posting.



This manuscript is a preprint and has not been peer reviewed. The copyright holder has made the manuscript available under a Creative Commons Attribution 4.0 International (CC BY) license and consented to have it forwarded to EarthArXiv for public posting.

Figure 2: National annual rainfall variability and drought thresholds in Kenya, 1991–2024.

Panels A–E display alternative transformations of the same national annual rainfall series; they are not independent tests. Blue denotes the separate 1991–1999 historical baseline (n=9), and orange denotes the 2000–2024 CHIRPS period (n=25). The vertical dashed line marks the January 2000 source transition. Panels F–H show source-era-specific P10/P20 thresholds and lower-tail classifications. Anomalies and thresholds are calculated separately for each source era; no pooled trend is estimated across the transition. The 1991–1999 segment is exploratory only.

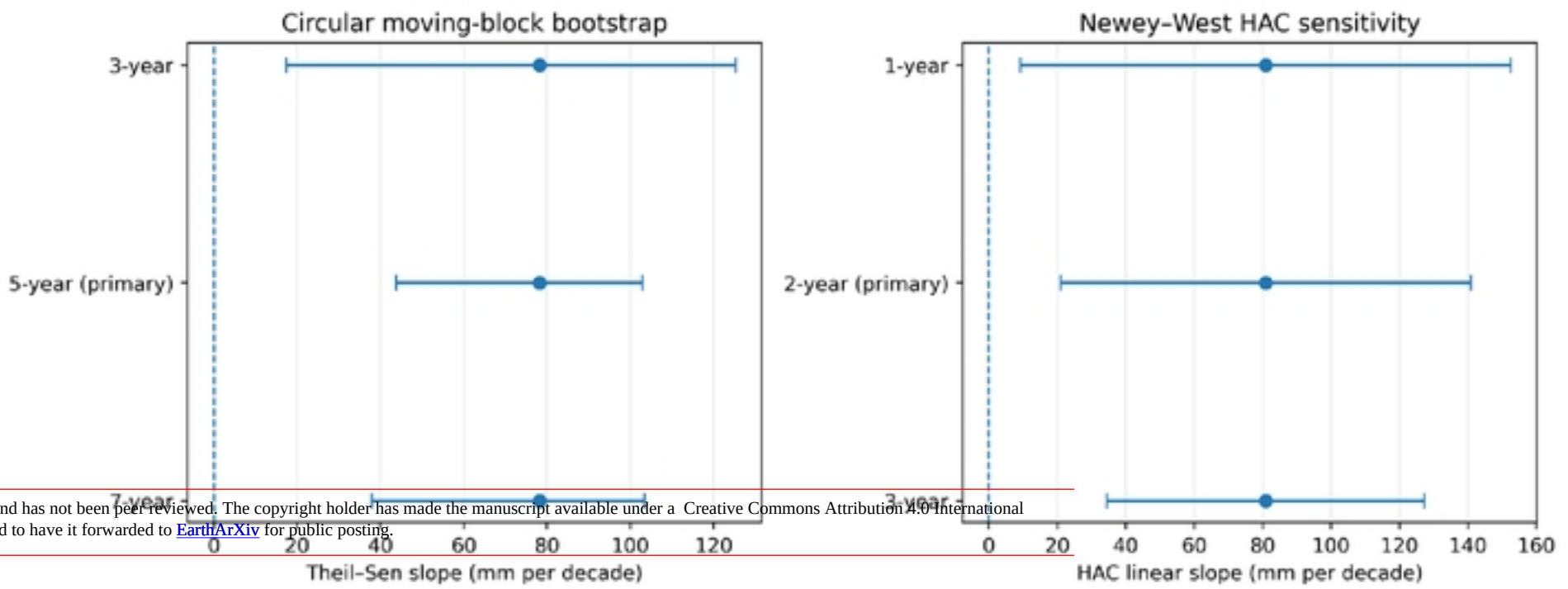


Figure 3: Theil–Sen confidence intervals under three circular block lengths and Newey–West HAC CI under three lag specifications

The point estimates are constant within each method because the same annual series and trend estimator are used; uncertainty changes with the dependence specification. All displayed intervals exclude zero

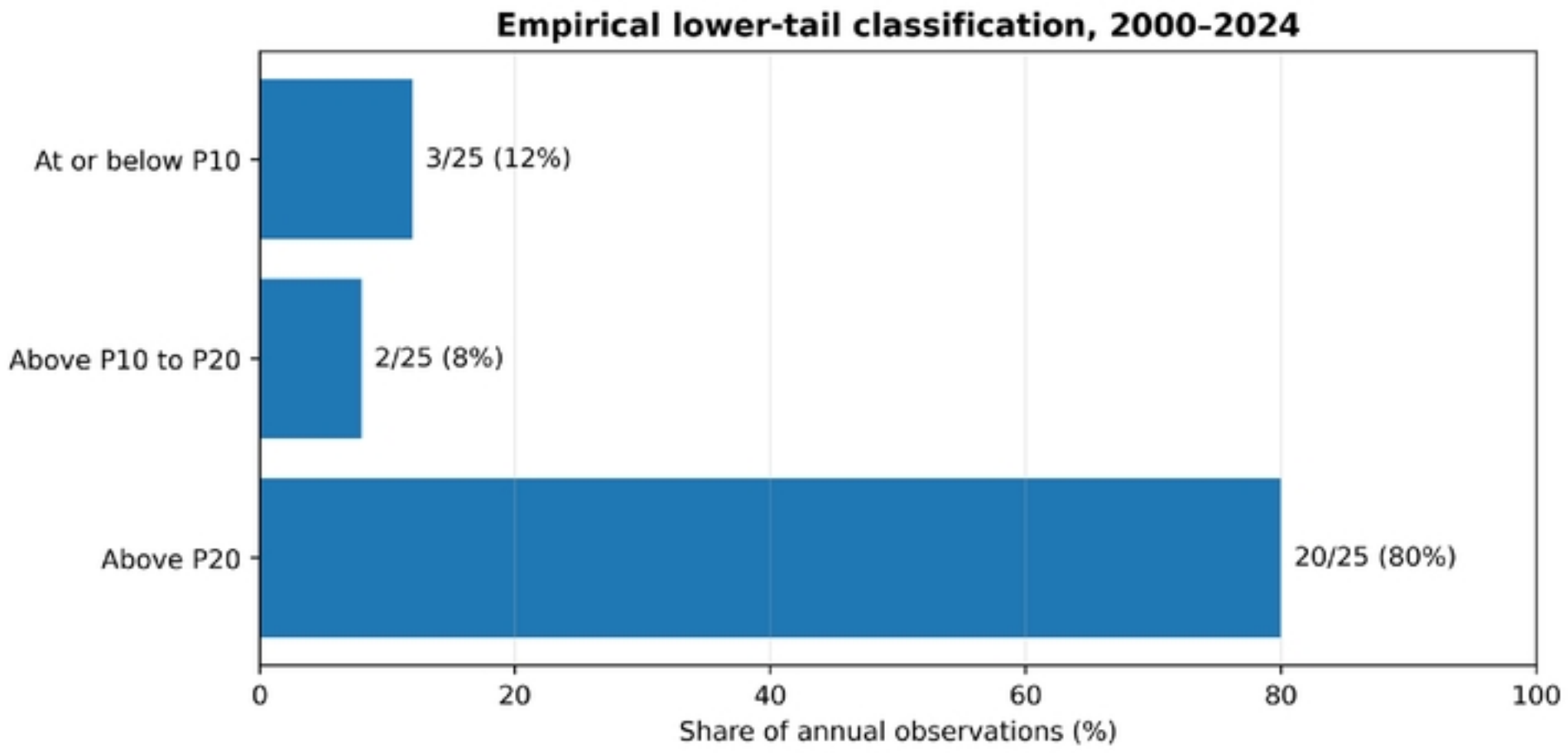


Figure 4: Distribution of annual rainfall observations across the three mutually exclusive empirical lower-tail categories

This manuscript is a preprint and has not been peer reviewed. The copyright holder has made the manuscript available under a Creative Commons Attribution 4.0 International (CC BY) license and consented to have it forwarded to EarthArXiv for public posting.

Kenya's annual and bimodal seasonal rainfall trends, 1991-2024



Era	Season	n	Sen slope	95% CBB CI	HAC p	Holm p	R^2
1991-1999	MAM	9	+50.8	-1.0 to +128.1	0.125	0.249	0.16
1991-1999	OND	9	+12.9	-106.1 to +152.2	0.417	0.417	0.02
2000-2024	MAM	25	+28.7	+7.6 to +40.8	0.027	0.053	0.12
2000-2024	OND	25	+14.7	-2.3 to +31.0	0.071	0.071	0.05

HAC reference df: 7 (1991–1999) and 23 (2000–2024).
Directional one-sided increase tests are a separate hypothesis analysis and are not mixed into this table.

Each source era is fitted independently. No pooled trend or cross-era hypothesis test. Axes are scaled independently by era.

Figure 5: Source-era-specific seasonal rainfall trends and relative MAM–OND accumulation in Kenya, 1991–2024

Figure 5 presents independent analyses of March–May (MAM) and October–December (OND) seasonal rainfall accumulation across two source eras: 1991–1999, based on the historical national rainfall source, and 2000–2024, based on CHIRPS national rainfall data. Each era was analysed independently, without pooling observations or undertaking formal cross-era hypothesis testing.

This manuscript is a preprint and has not been peer reviewed. The copyright holder has made the manuscript available under a Creative Commons Attribution 4.0 International (CC BY) license and consented to have it forwarded to EarthArXiv for public posting.

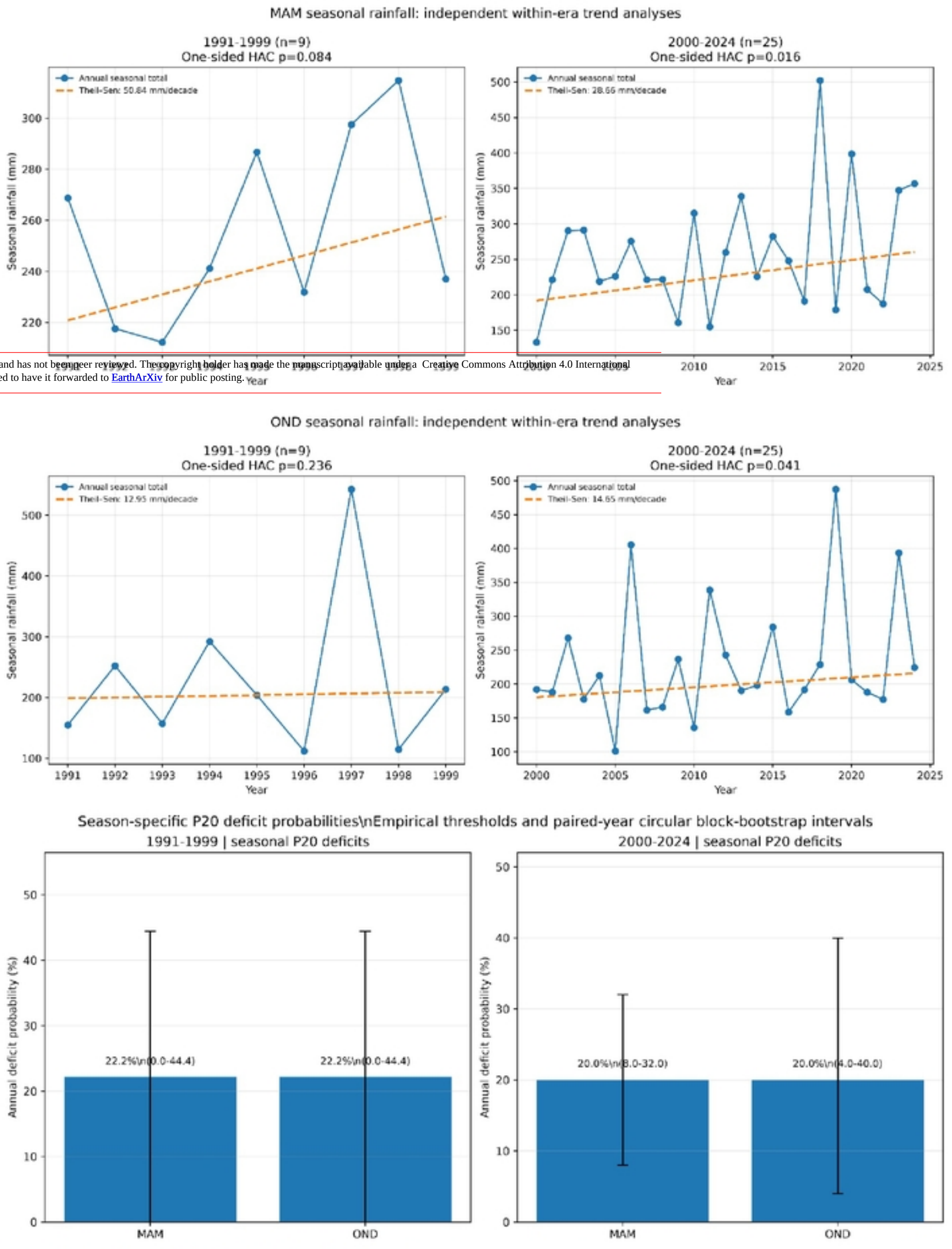


Figure 6: Season-trends and specific P20 rainfall deficit

This manuscript is a preprint and has not been peer reviewed. The copyright holder has made the manuscript available under a Creative Commons Attribution 4.0 International (CC BY) license and consented to have it forwarded to EarthArXiv for public posting.

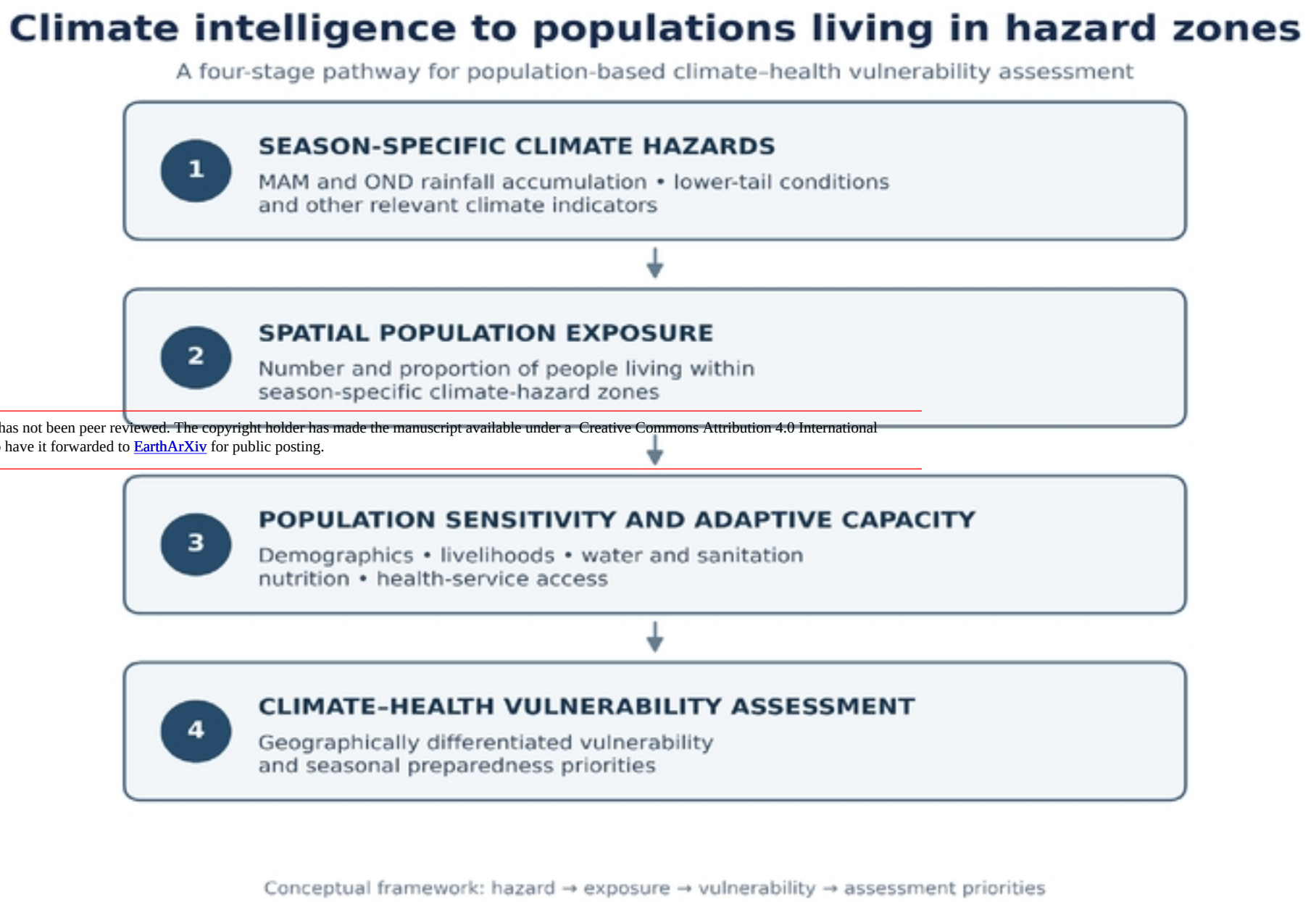


Figure 7: Conceptual steps from climate intelligence to implementation science

This manuscript is a preprint and has not been peer reviewed. The copyright holder has made the manuscript available under a Creative Commons Attribution 4.0 International (CC BY) license and consented to have it forwarded to EarthArXiv for public posting.